Signal overlap for elastic optical networks

Signal Overlap for Elastic Optical Networks

Tommaso Foggi, Filippo Cugini

***Abstract*—In Elastic Optical Networks (EONs), advanced transmission techniques based on coherent detection strategies have been proposed and exploited to provide high flexibility in resource allocation. So far, these techniques have assumed the constraint of each optical signal being transmitted along a dedicated frequency slot, by carefully avoiding frequency overlap with other optical signals.**

In this study, an overlap technique, that enables uncorrelated optical signals to be superimposed along the same spectrum resources, is designed and validated through simulations, both in terms of performance bounds and bit-error rate (BER) in coded transmissions. In particular, it is demonstrated how this technique allows each overlapped signal to be correctly received and detected. The proposed technique is less spectrally efficient and more complex to implement than increasing the constellation size and using non overlapping frequency slots, but it warrants consideration for flexible networking.

The proposed technique is first theoretically detailed and justified. Then, networking scenarios and implementation schemes suitable for its effective utilization are identified and applied in the case of two overlapped 112 Gb/s polarization-multiplexed quadrature phase shift keying (PM-QPSK) signals. Simulation results show that, applying 3-dB optical signal-to-noise ratio margin on the achieved bounds, optical reaches of around 800 km can be successfully supported by the proposed overlap technique.

Keywords*—*EON, RSA, routing and spectrum assignment, overlap, LDPC, defragmentation, reoptimization, flexi-grid, power.

I. Introduction

THE recent evolution of optical networks has been driven by the introduction of advanced transmission techniques based on coherent detection strategies [1]–[4]. Complex modulation formats (e.g., polarization multiplexed quadrature phase shift keying, PM-QPSK) and effective coding solutions [5], [6] have been successfully demonstrated, showing remarkable performance in terms of transmission efficiency. This efficiency has been effectively exploited through the adoption of the recently introduced flexi-grid technology, which enables the reservation of a configurable amount of spectrum resources. This way, the frequency range allocated to an optical signal, called frequency slot, can be configured to occupy only the minimum required amount of resources. The frequency slot is currently defined as the frequency range allocated to a slot within the flexible grid and *unavailable* to other slots [7], [8]. That is, so far, an optical signal has been considered to occupy a dedicated frequency range, with no sharing of spectrum resources with other independent optical signals, such as those generated by different source nodes. Indeed, so far, optical transmission systems have been designed and deployed in such a way that signal overlap among independent signals is avoided, so that only one optical signal per optical receiver is envisaged.

In this paper, a novel transmission technique enabling signal overlap is theoretically detailed and assessed, in order to support the design of a new set of optical network use cases.

This technique is inspired and supported by network information theory considerations, and specifically by the *multiple access channel* (MAC) topic (see [9, Ch. 14]), upon which solutions for the 5^{th}-generation of mobile communication systems have been also proposed [10]. Indeed, theory states that overlapped channels transmitted to a common receiver entail no mutual information reduction, as long as the first channel is detected and properly removed from the incoming signal, before detecting the second channel, and provided that the code rate and power of the two signals are selected according to the multiple access region specifications [9]. Thus, the performance that can be achieved in the context of optical networks will be shown.

In the literature, other kinds of signal cancellation techniques have been proposed for optical networks, as in [11], where the focus was on add/drop operations. In [11], a subcarrier is digitally isolated, converted back to optics, and interferometrically subtracted by destructive interference. That is, no digital processing is performed and no detection of overlapped signals is considered. On the contrary, we introduce a complete digital processing with the aim of allowing an effective detection of frequency overlapped signals. More specifically, the proposed technique is practically elaborated upon the work in [12], [13], and based on advanced coding technology, successive interference cancellation (SIC) strategies and proper configuration of optical transmission parameters.

The feasibility of the proposed overlap technique has been already successfully verified in an experimental work reported in [1], or, in a different version, in [14]. However, these works do not include theoretical details and do not provide assessments in terms of expected optical reaches.

The overlap technique does not require global time or frequency synchronization in the whole network. Moreover, the technique does not rely on orthogonal codes as in Optical Code-Division Multiple-Access (O-CDMA) solutions [15], [16]. Instead, in this study we specifically consider the overlap of two uncorrelated optical signals, which may be generated, at the same central frequency, even from two different and independent network nodes. In this light, it is clear that other, even more sophisticated, multiuser techniques (e.g. [17]) are not suitable for our purposes, since they typically involve complex processing, beside the one we propose, and rely on synchronization requirements that severely limit their feasibility. Alternatively, there exist many examples of simple multiple-input multiple-output (MIMO) processing, see [18], [19], but if actual multiuser detection is not envisaged, as in these cases, the performance penalty is excessive. Indeed, these works do not target fully overlapped signals. For example, in [19], the central frequencies of two 10-GBaud PM-QPSK signals remain separated by 6 GHz.

T. Foggi (email: tommaso.foggi@cnit.it), F. Cugini are with CNIT, Italy. This paper is an extended version of the work presented in [1]. This work was partially supported by the IDEALIST project and by the Italian Ministero dell'Istruzione, dell'Università e della Ricerca (MIUR) under the FIRB project Coherent Terabit Optical Networks (COTONE).

We here present results on symbol-by-symbol memoryless detector, but it is worth noting that this technique can be also applied to time-frequency-packing (TFP) systems (see [20]) by employing a maximum *a-posteriori* probability (MAP) symbol detector [21]. Moreover, we chose the PM-QPSK modulation format, as it is nowadays the most popular one in commercial systems, but similar considerations could be derived for higher-order modulation formats. Indeed, the purpose of the proposed technique is not the spectral efficiency increase, rather it is designed to provide possible advantages from the enabled operations related to networking issues. Clearly, our purpose is to show that it is possible to receive two overlapped signals transmitted by two different nodes, and in this sense the joint transmission of both signals employing higher-order modulation formats is left for future work.

In this study, for the first time, the overlap technique is theoretically described in the context of optical networks.

Then, numerical evaluation of achievable bounds (AB) on the net bit rate are proposed and reported, by resorting to the simulation-based technique in [22], [23]. The computed bound can be efficiently exploited to guide the estimation of parameters like required optical signal to noise ratio (OSNR) and power ratio between the overlapped channels. Then, bit-error rate (BER) simulations of practical low-density parity-check (LDPC) codes, as in [13], are used to confirm the behavior of the theoretical predictions. Thus, the overlap of two 112 Gb/s PM-QPSK is assessed in terms of OSNR performance, showing the achievable working conditions and the LDPC codes to be adopted.

The proposed technique is less spectrally efficient and more complex to implement than increasing the constellation size and using non overlapping frequency slots, but it targets different use cases for flexible networking. In fact, the technique opens the way for new networking solutions. Specifically designed routing and spectrum assignment (RSA, [24], [25]) strategies can be introduced to exploit the signal overlap. Moreover, new recovery strategies can be considered. For example, at the destination node, the overlap technique enables a transponder dedicated to a specific lightpath to be also utilized as backup of a different card and lightpath, thus limiting the equipment of spare additional transponders. Furthermore, new de-fragmentation schemes can be considered, such as the hitless shifting through push-pull [26], enhanced by the capability to perform signal overlap. Indeed, it is worth noting that signals can also be only partially overlapped and their frequency offset can be safely tracked.

The overlap technique requires additional processing capabilities with respect to currently available receiver solutions. Moreover, such processing introduces, at the receiver, additional latency on one of the two overlapped signals. These aspects have to be accounted for in the definition of the possible networking applications. However, it is important to consider that, as occurred for wireless transmission techniques in the latest years, the evolution of processing capabilities will relax such limitations, so that the implementation of more advanced optical transmission techniques will be simplified and enabled.

In this work, we identify possible practical use cases for this technique. For space reasons, their detailed definition and evaluation, as well as the accurate assessment of the aforementioned limitations, is left for future dedicated works.

In this paper we focus on: (1) demonstrating, from a theoretical perspective, the feasibility of the signal overlap technique in the context of optical networks, (2) the assessment of the transmission performance on practical optical network scenarios.

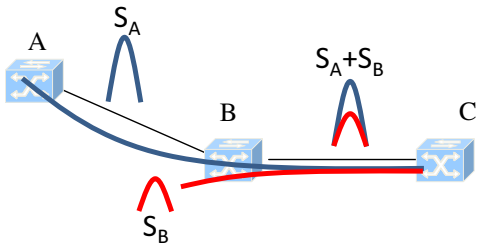

Figure 1. Example of Overlap technique applied on a reference network scenario.

II. Technique for Signal Overlap

A. Working principle

The overlap technique is designed to allow two independent optical signals S_A and S_B to be modulated and transmitted over the same optical spectrum resources and to be correctly received and detected.

Fig. 1 shows a schematic reference network scenario where the overlap technique is applied. To stress the independency between the two signals (i.e., no orthogonal codes or synchronization are adopted), the reference scenario considers the two signals generated from two disjoint nodes. Signal S_A is transmitted by node A at central frequency f_o over link A-B. Signal S_B is transmitted by node B at the same central frequency f_o. At node B, the two signals overlap. They are then jointly propagated along B-C towards the common receiver in node C, where coherent detection is exploited. Notice that node B can lie anywhere over $A-C$, in the sense that signals can jointly propagate from any distance, *without synchronization requirements*. For the same reason, also notice that signal S_B may also be generated by a different remote node and propagated before the overlap. Indeed, despite the signal superposition, our technique allows to correctly detect both overlapped signals.

The signal superposition relies on properly designed transmission parameters such as the mutual power level and the LDPC code applied to each of the two signals. In particular, before they overlap, the power of the modulated signal S_B is properly set to a value lower than the power of S_A. Moreover, the code rates used to encode S_A and S_B are properly chosen in order to have adequately robust transmissions.

At the receiver (node C), after the coherent opto-electronic conversion of the *overall* signal S_A+S_B, sampling and digital processing (DSP) are performed.

As a first step, the detection is performed as if only S_A were transmitted, i.e., considering S_B simply as interference. This way, the coded signal S_A is retrieved from the acquired data. Then, at a later stage, the acquired data are reprocessed to perform the cancellation of signal S_A, as will be explained in details in the following. Once the cancellation is complete, a second detection stage is performed on the interfering coded channel S_B.

By properly exploiting code rates and power levels as adjustable parameters, it is possible to design a transmission system that allows the detection of overlapped independent

signals with achievable rates depending on the particular conditions.

Notice that, in the light of the network scenario here considered, any technique based on actual MIMO processing is unfeasible, because it would entail a joint and synchronized signal transmission.

The technique was derived from the wireless technology (see [12] and references therein, targeting spectral efficiency optimization purposes), while here it is specifically detailed for the first time in the context of optical transmissions.

In order to ease the comprehension of the system at hand, a few basic concepts are first introduced. The analysis is mainly driven by results on the information rate, derived, as already stated, by exploiting the *auxiliary channel* method and the principle of *mismatch detection* (see [20], [23]). As an example, consider Fig. 2a where it is represented the net bit rate of S_A transmitted alone, computed from the achievable information rate bound, as a function of OSNR, and, in contrast, the net bit rate of S_A and S_B as a function of the carrier to interference ratio C/I, i.e., the relative power between the two channels, as explained in the following, in the absence of noise, in Fig. 2b. In this case, S_A is first detected by considering S_B as a simple noisy interference, then the received signal is processed as to obtain proper estimates, including impairments, that allow the re-modulation of signal S_A, in order to subtract it from the received signal, so that S_B can be ideally detected without interference. Clearly, in a realistic scenario two main drawbacks must be taken into account: first, the re-modulation of S_A has necessarily a limited accuracy, as some impairments are difficult to be estimated (e.g. non-linear effects); second, the detection of S_B will be also affected by the noise from the S_A lightpath. Thus, these two effects will further impair the performance of the second channel detection. However, by combining the two explained scenarios, it is possible to draw a contour plot as a function of S_A OSNR (expressed as $OSNR_{S_A}$ in figures) and C/I, that stresses the net bit rate of both channels, as shown in Fig. 3. Notice the the results of Fig. 2a can be considered as the asymptotic results of Fig. 3 when C/I goes to infinity (upper side, S_B is clearly not present), whereas the results of Fig. 2b can be sketched for OSNR going to infinity (right side) in Fig. 3. In this latter case it must be considered that the performance of S_A increases monotonically as a function of C/I, whereas S_B has an opposite dependence on C/I, but it is only slightly influenced by the presence of S_A, at least for the evaluated values of C/I. In Fig. 3, each solid line refers to a specific achievable bound of signal S_A overlapped with S_B. Thus, each solid line allows to derive the C/I and S_A OSNR for the related value of the achievable bound. Similarly, each dashed line allows to derive the C/I referred to S_A OSNR required to achieve the related achievable bound of S_B. Clearly, the intersection between a solid and a dashed line provides the minimum OSNR value required to successfully achieve the related bit rates on both signals.

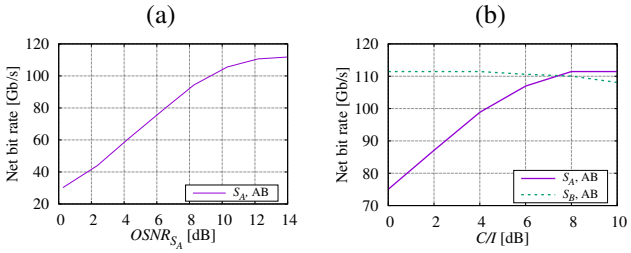

Figure 2. Net bit rate achievable bound (AB) of a) signal S_A alone as a function of its OSNR and b) S_A and S_B as a function of relative power C/I in the absence of noise.

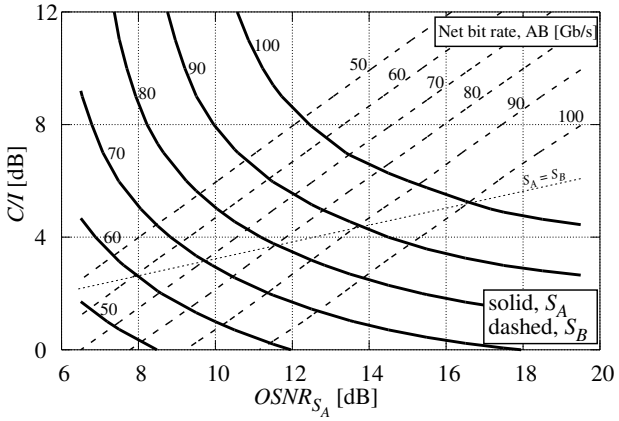

Figure 3. Contour plots of net bit rate AB for channels S_A and S_B, as a function of C/I and S_A OSNR (gross rate R=112 Gb/s).

B. Network scenarios and possible use cases

The proposed overlap technique can be suitably considered for different future networking scenarios and use cases.

A first possible scenario is the innovative Drop and Waste (D&W) metro network architecture (also called filterless) described in [27]. The D&W architecture has been experimented by Croatian Telecom considering an horseshoe topology, as the one in Fig. 1 [28]. In D&W, only splitters/couplers and amplifiers are utilized, without relying on expensive reconfigurable optical add-drop multiplexers (ROADMs). Indeed, thanks to the coherent technology, each transmitted signal can be properly selected at the receiver. In D&W, as a major drawback, a waste of spectrum resources is experienced since each signal occupies the entire horseshoe network. However, significant capital and operational expenditure (CapEx, OpEx) savings are expected thanks to the lack of ROADMs and their control and maintenance operations. The proposed overlap technique can be implemented in a D&W horseshoe topology, as the one in Fig. 1, by properly configuring the power levels at the transmitters according to the power levels expected at the superimposition point (i.e., the coupler at node B).

A second possible networking scenario is a ROADM-based metro network employing the new generation of wavelength selective switches (WSSes) [29]. These new WSSes, besides the ability to direct different portions of the spectrum to different output ports, also support power splitting/coupling over different ports, with adjustable attenuation capabilities. For example, with reference to Fig. 1, this WSS employed at the superimposition point (i.e., within node B) would be configured to allow both ports receiving signals S_A and S_B to couple the frequencies around f_0 in the output port towards node C (with signal S_B properly attenuated).

In the context of either D&W (filterless) or ROADM-based optical network scenarios, several use cases can be identified. Two examples are here highlighted.

- *Defragmentation*. Fig. 4a shows a fragmented spectrum scenario. In particular, signal S_B added at central frequency f_{-1} on link B-C is contiguous to a pass-through lightpath S_A occupying central frequency f_0 on

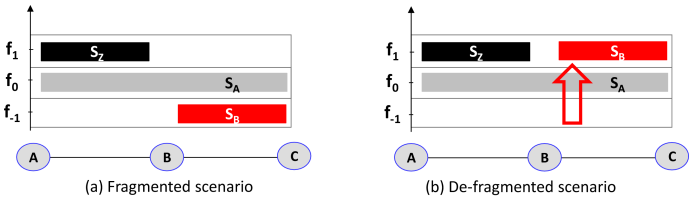

Figure 4. Example of defragmentation use case.

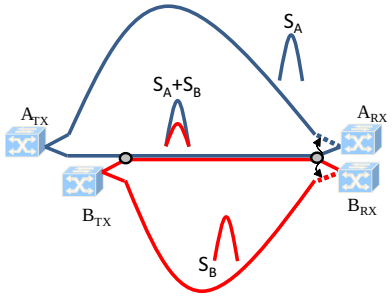

Figure 5. Example of 1+1 protection exploiting overlap.

links A-B-C. At central frequency f_1 no channels are present on link B-C, leading to a fragmented condition given the presence of a third signal S_Z on link A-B. Fig. 4b shows the spectrum scenario targeted by the defragmentation procedure, where signal S_B now appears at central frequency f_1 on link B-C. Such defragmentation cannot be achieved by relying on a conventional approach of increasing the constellation size with non overlapping frequency slots. Instead, it may be achieved by performing hitless shifting through push-pull technique [26], enhanced by the capability to perform signal overlap. Notice that in this study we do not claim this defragmentation procedure is feasible (a dedicated study is needed). Instead, we claim that to target the implementation of such defragmentation procedure, successful detection of overlapped signals has to be guaranteed.

- *Recovery*. A first use case in the context of recovery is to address card failures. Two independent signals, under normal conditions, are received by two different receivers at the same destination node. The overlap technique enables each receiver to be also utilized as backup of the other one, thus increasing the overall availability or limiting the equipment of spare additional cards. A second use case for recovery occurs in case of link/node failures where spectrum continuity constraints may prevent the recovery of some signals. In this case, a number of such signals may also exploit the signal overlap, improving the chance to partially or fully recovering the failed traffic. A third use case refers to 1+1 protection where the transmitted signal is split along both a working and a backup path (Fig. 5). In the case the longer protected path requires robust transmission (e.g., PM-QPSK), a more efficient PM-16QAM format can not be utilized on the (shorter) working path, given the simultaneous transmission on both paths. This provides the availability of high margin in the working path. In such a use case, signal overlap with a different working path heading the same destination may be implemented, providing potential efficiency not achievable with other conventional approaches.

As anticipated, additional and specific investigation is required to actually confirm the real benefit of applying the proposed overlap technique in these scenarios and use cases. However, before addressing such use cases, it is mandatory to assess the theoretical feasibility of the overlap technique, as per the objective of this paper.

C. Detailed description

Two independent PM-QPSK[1] signals S_A and S_B are coded (at code rate r_A and r_B respectively) and transmitted at the same central frequency f_o

The code rate r is here expressed in the form i/j: i bits of data and $(j$-$i)$ bits of overhead out of the j transmitted. The transmitted net bit rate is then obtained multiplying the gross rate R with the code rate i/j. For example, a 9/10 code rate r provides a net bit rate I of about 100 Gb/s (100.8 to be exact) when a gross rate R of 112 Gb/s is considered.

Proper power levels are set before overlap, such that the power of S_A is typically higher than the one of signal S_B. This way, considering at first S_A as useful signal and S_B simply as interference, S_A experiences a specific carrier to interference (C/I) power ratio at the receiver.

At the receiver, coherent detection is applied on (noisy) signal S_A+S_B, applying analog to digital conversion and DSP.

The DSP follows the system schematically depicted in Fig. 6. It includes: sampling, that provides two samples per symbol; an optional (on short links it may not be necessary) chromatic dispersion compensation through a fixed tap equalizer; frame synchronization, aimed at identifying a properly designed reference header, namely a bit pattern, also in presence of uncompensated polarization rotations, frequency offset, phase noise, and unknown inter-symbol interference; frequency synchronization, that compensates for the frequency mismatch between the incoming signal and the local oscillator (see [30]); a two dimensional adaptive fractionally-spaced feed-forward equalizer (2D-FFE) that compensates for linear propagation impairments, like group velocity dispersion (GVD) and polarization mode dispersion (PMD), and performs polarization demultiplexing, with taps updated by the minimum mean square error (MMSE) algorithm, since the system is designed to allow, possibly, the time-frequency packing principle [20]; advanced phase error estimation (more accurate than a simple phase locked loop), by exploiting initially the presence of 1% of pilot symbols, in order to compensate for the phase noise due to the local oscillator (LO);[2] finally, decisions on transmitted symbols are taken in the following iterative LDPC decoder, whose iterations clearly introduce latency on the detection of codewords. The decoding stage can possibly take advantage of a MAP symbol detector working on a trellis, as in [20], depending on TFP principle is exploited or not, as it would entail the introduction of intersymbol interference (ISI), which must be coped with by a proper detector. The results reported in this work were obtained without resorting to a MAP detector.

The detection is performed according to the following steps. First, only signal S_A is detected, considering S_B as

[1]We remind that any other modulation format could be employed, in principle. As regard to the comparison between different modulation formats in terms of spectral efficiency, please see [22].

[2]Results reported in Sect. III include the presence of the pilot symbols and the reference header in the computation of the actual bit rate.

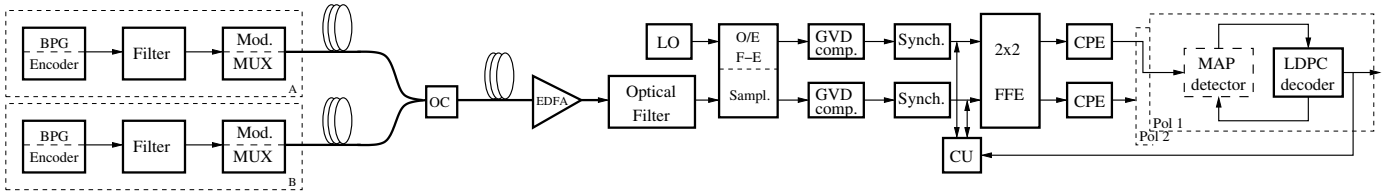

Figure 6. System model. BPG: bit pattern generator, MUX: multiplexer, OC: optical combiner, EDFA: erbium-doper fiber amplifier, LO: local oscillator, O/E F-E: opto/electrial front-end, GVD comp.: group velocity dispersion compensation, FFE: feed-forward equalizer, CU: cancellation unit, CPE: carrier phase estimation, MAP: maximum a-posteriori probability, LDPC: low-density parity-check.

interference. Second, the recovered data stream is re-used to estimate signal impairments and propagation parameters, which allow the (best possible) cancellation of the signal S_A from the acquired one. Once the cancellation is complete, further processing is performed to detect the coded channel S_B. It is worth noting that, in addition to the latency due to the first channel decoding, a further delay must be envisaged because of the cancellation processing, in order to enable the detection of the second channel. On the other hand, some processing is saved, e.g. GVD can be compensated for once for both channels, at least for the shortest propagation length, and frequency offset estimation for S_B can take advantage of the previous estimation on S_A.

Since two overlapped independent signals are received, particular attention has to be paid to the frame and frequency synchronization processing performed in the DSP, that proceed as follows. The signal is digitally filtered with a 4^{th}-order Gaussian filter to remove out-of-band residual noise. A short known header (448 bits) is looked for in the received sample sequence, and then used for an initial rough estimation of the frequency offset, in case of cold acquisition, i.e., at transmission start-up.[3] Once the first frequency estimation is available, it is possible to identify the transmitted symbol sequence and exploit the first transmitted code word to perform a fine frequency estimation (as concerns the simulated system). Both estimation steps are based on the algorithm in [31]. Once the offset is acquired, its slow variations can be followed by simpler algorithms, as in [26]. After that, equalization and polarization demultiplexing is performed by the adaptive 2D-FFE with 17-taps, whose adaptation exploits the first known codeword at system start-up (whereas decisions are used in the following), and then decisions are taken by the iterative LDPC decoder.

Then, a key role is played by the SIC stage. For ease of comprehension, we briefly recap the system analytical model. From nodes A and B two PM-QPSK signals are launched on orthogonal polarizations x, y, whose expression is[4]

$$\left[s_x^{A(B)}(t)\ \ s_y^{A(B)}(t)\right]^T = \sum_k \mathbf{c}_k^{A(B)} \mathbf{P}^{A(B)}(t-kT), \qquad (1)$$

where T is the symbol interval, $\mathbf{c}_k = [c_{x,k}\ \ c_{y,k}]$ are symbols belonging to a generic M-ary complex alphabet (in our case QPSK), derived from the LDPC encoding of a sequence of message bits, and $\mathbf{P}(t) = p(t)\mathbf{I}$ where $p(t)$ is the transmitting pulse (notice that it can be different for S_A and S_B) and $\mathbf{I}$ is the 2×2 identity matrix. From (1) descends the general expression of the received signal

$$\begin{aligned} \mathbf{r}(t) &= [r_x(t)\ \ r_y(t)]^T = \mathbf{z}^A(t) + \mathbf{z}^B(t) + \mathbf{w}(t) \\ &= \gamma \textstyle\sum_k \mathbf{c}_k^A \mathbf{Q}^A(t-kT-\tau_A) e^{j(2\pi F_A t + \theta_A)} \\ &+ \sqrt{1-\gamma^2} \textstyle\sum_k \mathbf{c}_k^B \mathbf{Q}^B(t-kT-\tau_B) e^{j(2\pi F_B t + \theta_B)} \\ &+ \mathbf{w}(t), \end{aligned} \qquad (2)$$

where $\mathbf{z}^{A(B)}(t)$ represents the signal components that can be estimated, $\mathbf{Q}^{A(B)}(t)$ is a 2×2 matrix given by $\mathbf{Q}(t) = \mathbf{P}(t) \otimes \mathbf{H}(t)$, $\mathbf{H}(t)$ representing the 2×2 channel impulse response (including linear impairments and filtering), γ is the power allocation factor, related to the carrier to interference ratio by $C/I = \gamma^2/(1-\gamma^2)$, that determines the power ratio between the two overlapped signals (which can be set at the transmitting nodes or at node C), $F_{A(B)}$ are frequency offsets with respect to the local oscillator (LO), $\tau_{A(B)}$ and $\theta_{A(B)}$ are initial delays and phases of the respective carriers, $\mathbf{w}(t) = [w_x(t)\ \ w_y(t)]^T$ is additive white Gaussian noise (AWGN), whose complex components has two-sided power spectral density (PSD) equal to N_0, and represents, with reference to Fig. 1, the sum of the noise from all signal paths. The expression of the signal from node A, that must be cancelled after detection, can be thus rewritten as

$$\begin{aligned} \mathbf{z}^A(t) &= \left[z_x^A(t)\ \ z_y^A(t)\right]^T \\ &= \textstyle\sum_k \mathbf{c}_k^A \mathbf{Q}^A(t-kT-\tau_A) e^{j(2\pi F_A t + \theta_A)}, \end{aligned} \qquad (3)$$

where γ has been assimilated in $\mathbf{Q}^A(t)$ for simplicity. The cancellation algorithm is therefore designed to estimate samples $\mathbf{Q}_k^A = \mathbf{Q}^A(t)|_{t=t_k}$, which includes time-invariants or slowly-varying channel effects and impairments, where t_k are the sampling instants, and the phase term, typically time-varying at fast rate, $\theta_A = \theta_A(t_k)$. Such algorithm must also be adaptive, evidently, in order to track channel changes, i.e., timing jitters, PMD, etc. Notice that the estimation of the frequency offset term F_A is already available, as it is initially performed in order to be removed from the signal before detection. The superscript A will be neglected in the following for simplicity. The estimation of channel impulse response samples is performed through a decision-directed MMSE algorithm (see [32]), delivering an estimate of the received signal samples, namely

$$\begin{aligned} \hat{z}_{x,k} &= \textstyle\sum_i \left(\hat{c}_{x,k-i}\hat{q}_i^{x,x} + \hat{c}_{y,k-i}\hat{q}_i^{x,y}\right) \\ \hat{z}_{y,k} &= \textstyle\sum_i \left(\hat{c}_{x,k-i}\hat{q}_i^{y,x} + \hat{c}_{y,k-i}\hat{q}_i^{y,y}\right), \end{aligned} \qquad (4)$$

where $i = 1, ..., N_E$, N_E being the number of taps of the 2×2 estimated impulse response $\hat{q}_i^{m,l}$, $m, l = x, y$, and the hat overscript denotes estimates. The channel coefficients update is then performed as

$$\hat{q}_i^{m,l,(k+1)} = \hat{q}_i^{m,l,(k)} + \alpha \cdot \left(\hat{z}_{m,k} - r_{m,k}\right) \hat{c}_{l,k-i}^*, \qquad (5)$$

[3]The local oscillator is not optically locked to the signal carrier.

[4]In the following, $(\cdot)^T$ denotes transpose, $(\cdot)^*$ complex conjugate, the bold font is used for vectors and capital bold for matrices. Superscripts A, B are omitted where unnecessary.

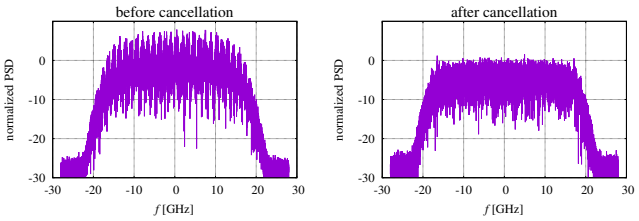

Figure 7. Received signal power spectral density before and after cancellation, C/I=10 dB.

being α a proper step-size. The estimate of the phase term is instead obtained through a sliding window average of proper length (in the order of tens of samples, depending on the particular evaluated scenario), by exploiting the received samples and the detected symbols filtered by the estimated channel taps, namely

$$\hat{\theta}^{(k+1)} = \tan^{-1}\Big(\sum_{\ell} r^{\bar{f}}_{m,k-\ell}\hat{z}^{*}_{m,k-\ell}e^{j2\pi\hat{F}}\Big), \qquad (6)$$

where, in this case, the received samples do not undergo frequency compensation (as denoted by the superscript $\bar{f}$), so that this estimate can be also exploited to recover the phase error due to imperfect frequency offset compensation.

Once the tributary $\hat{\mathbf{z}}^{A}_{k} = \hat{\mathbf{z}}^{A}(t)|_{t=t_k}$ has been completely estimated, it can be used to cancel the signal transmitted by node A in $\mathbf{r}_k = \mathbf{r}(t)|_{t=t_k}$ from (2), thus allowing the processing and detection of the signal from node B.[5] Clearly the noise from eq. (2) cannot be cancelled, and thus, even if assuming a perfect cancellation of signal S_A, the noise at the receiver is the noise from both signal paths. However, its effect is accounted for in the results presented in next section.

We would like to point out that the presented cancellation algorithm represents one of the possible solutions that can be implemented with similar performance. The advantages of the proposed technique lie in the straightforward and flexibile optimization, since we found that an α parameter equal to 10^{-4} is optimal in a wide range of cases, just as a sliding window length equal to 40 symbols. Moreover, we did not elaborate on the influence of detection errors on the cancellation performance, since our simulations deal with coded transmissions, so we assumed perfectly decoded bits; however, we verified that a BER in the order of 10^{-5} did not entail any worsening. Even though we did not take on an accurate analysis, the effects of decision-feedback processing for uncoded transmissions have been widely analyzed in literature (e.g., see [33]).

Fig. 7 shows an example of the received optical PSD before and after cancellation. In this case, C/I=10 dB is reported.

III. Numerical results

The two independent signals S_A and S_B were considered as LDPC coded PM-QPSK signals at gross bit rate R. A value of R=112 Gb/s was first assumed for both S_A and S_B (i.e., R_A=R_B=112 Gb/s). A tributary traffic was targeted at a bit rate of 100 Gb/s, and linear regime was assumed (i.e., the link is essentially an AWGN channel) at first.

In the simulations, an analog to digital converter (ADC) with an analog bandwidth of 20 GHz and a sampling rate of 56 GSample/s was assumed. Both signals were filtered at transmitter and receiver side with 4^{th}-order Gaussian optical filters, whose 35-GHz bandpass bandwidth (BW) enabled to fit the requirements of a 37.5 GHz flexi-grid network scenario. This way, no detrimental filtering affected the transmission performance.

Parameter	value	Parameter	value
Symbol rate	28 Gbaud	LO linewidth	100 kHz
ADC BW	20 GHz	Max freq. offset	2 GHz
ADC resolution	8 bits	AB simulated bits	$\sim 10^6$
Tx,Rx filter type	4^{th} Gauss.	LDPC simulated bits	$\sim 10^7$
Tx,Rx filter BW	35 GHz	BER threshold	$\sim 10^{-4}$

Table I. Back-to-back simulation parameters.

The performance of the overlap technique was then evaluated by configuring code rate and power levels. When adequate OSNR performance was experienced and a code rate of $9/10$ was applied, the net bit rate I of about 100 Gb/s was successfully provided to the receiver.[6] On the other hand, when adequate OSNR performance was not guaranteed, a more robust code rate had to be applied. For example, a code rate of $4/5$ on the same rate R provides a net bit rate I of around 90 Gb/s. Two different schemes were then considered. The first scheme assures a net bit rate of S_A equal to the required I_A=100 Gb/s, and targets the maximization of the net bit rate of S_B. In this case, the whole amount of tributary traffic in S_A was assured and only signal S_B admitted a reduced net bit rate (i.e., $I_B \leq$100 Gb/s). The second scheme targeted the maximization of the overall bit rate, i.e. the sum of the net bit rate I_A+I_B of the two overlapped signals S_A and S_B. In this case both signals could be configured with a bit rate lower than 100 Gb/s (i.e., $I_A \leq$100 Gb/s, $I_B \leq$100 Gb/s).

The performance of the system was then evaluated as a function of C/I and $OSNR_{S_A} = 10\log_{10}(P_A/P_{ASE})$[7], where P_A is the power associated to channel S_A and P_{ASE} was the amplified spontaneous emission (ASE) noise power due to optical amplifiers, measured on a 0.1 nm bandwidth, and referred to the propagation of S_A alone.

A back-to-back scenario was first considered, thus the two signals are just overlapped at transmitter side, then noise is added before detection. Fig. 3, already introduced in sect. IIA, shows the main simulation results of the presented work, namely the net bit rate achievable bounds of signal S_A and S_B as a function of S_A OSNR and C/I, which entails the S_B OSNR; these bounds were theoretically computed by exploiting the principles in [23] (see also [13], [20] for details) to determine the average mutual information per symbol, successively multiplied by the nominal bit rate R.

For every scenario, the system was entirely simulated, from signal propagation to transmit and receive side attributes. In case of net bit rate computation, the processed signal samples instead of feeding the decoder, were used to compute the achievable information rates, through the proper numerical method; in case of codes simulations, the samples were processed iteratively by the decoder.

The following figures will prove the good matching between the computed bounds and the LDPC codes simulations.

The presented results on the achievable bound were obtained by Monte Carlo simulations of 10^6 bits per point, and approximately one point per half dB of C/I and OSNR, and then the derived contour plots were smoothed with a worst-case

[5]Notice that we verified that such processing does not entail any additional quantization issues with respect to the standard receive side processing, as 7-8 bits are sufficient to avoid any penalty.

[6]Including the presence of pilot symbols and the codeword header, the actual net bit rate is 99.6 Gb/s.

[7]The same definition applies also to channel S_B.

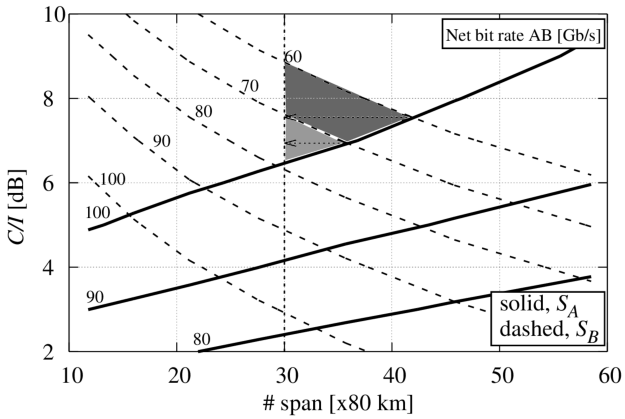

Figure 8. Contour plots of net bit rate AB for channels S_A and S_B, as a function of C/I and number of spans (gross rate R=112 Gb/s).

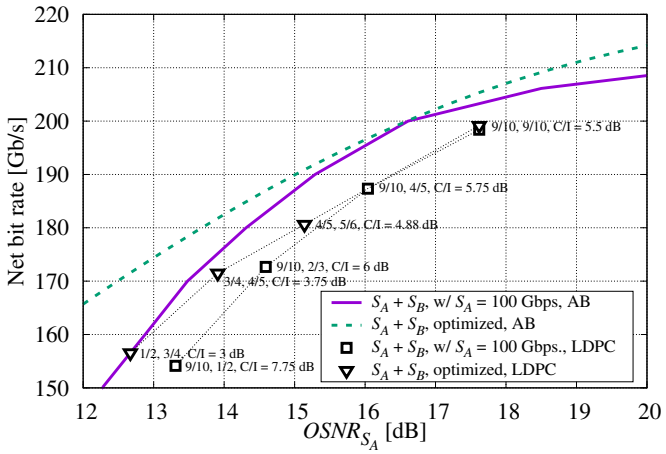

Figure 9. Net bit rate AB for channels S_A and S_B when S_A is fixed to 100 Gb/s and when the overall bit rate is optimized, and LDPC codes simulations.

relative error of less than 4%. The main simulation parameters are summarized in Table I. As already highlighted, Fig. 3 shows the main results as concerns the proposed technique; it can be noticed that, actually, it is always possible to detect two overlapped signals, so that, given C/I and OSNR, a certain overall bound on the bit rate can be determined. Such characterization of the working points can be performed on real links through experimental data (thus also including nonlinear effects), in order to identify, and possibly design, proper codes that allow the transmission in given scenarios, which depend on link parameters, i.e. span lengths, position of add/drop nodes, amplification, etc. The outcome of Fig. 3 can be easily converted into link reaches, once the OSNR characterization of the link is known, that is, on an actual link the spectral efficiency bounds can be computed at a given link distance, to which a measured OSNR corresponds, and they can be expressed as a function of one parameter or the other. As an example, consider Fig. 8: we converted the OSNR into reach for an arbitrary link (we just used as a reference the link we used in the simulations of Figs. 12-13, described in the following). It can be seen from figure that, for example, if we want to guarantee 100 Gbps for S_A, we must consider the grey-shaded region above the solid curve labelled with '100', and we are thus forced to lower the net bit rate of S_B below 80 Gbps. So we can try to use, or design, a code for S_B (we consider in this case a rate 9/10 code for S_A) that fits the light grey region, i.e. for a 70 Gbps net bit rate, or, at worst, for 60 Gbps (light and dark grey regions). Depending on the necessary margin, we should be able to reach 30 spans with C/I around 8 dB, a 9/10 code for S_A and a code in the range 2/3÷3/5 for S_B.

Fig. 9 shows the performance of the proposed overlap technique expressed as the sum of the net bit rate achievable bound of both channels (i.e., I_A+I_B) as a function of the S_A OSNR. In particular, the solid curve here reports on the performance when the net bit rate of S_A is fixed to 100 Gbit/s, whereas the dashed one refers to the case of maximization of the overall net bit rate of $S_A + S_B$. The two curves match for S_A OSNR equal to $OSNR_{100}$=16.5 dB. This $OSNR_{S_A} = OSNR_{100}$ value corresponds to the minimum OSNR enabling a working point where each overlapped channel successfully guarantees the requested bit rate of 100 Gb/s. The additional net bit rate potentially achievable for higher OSNR values (i.e., larger than $OSNR_{100}$ where I_A+I_B>200 Gb/s) is not actually exploitable given that each tributary operates at 100 Gb/s. For OSNR values lower than $OSNR_{100}$, a degraded scenario was experienced. Results show that the scheme targeting the maximization of the overall bit rate guarantees better performance compared to the other scheme where I_A is kept fixed to 100 Gb/s. For example, I_A+I_B=180 Gb/s is achieved for S_A OSNR equal to 14.3 dB in the latter case, and equal to 13.7 dB in the maximized scheme. The difference between the two schemes becomes rather relevant for OSNR values significantly lower than $OSNR_{100}$. However, particularly for OSNR values slightly lower than $OSNR_{100}$, limited difference is experienced between the two schemes. For example, with S_A experiencing an OSNR of 14 dB, the values of I_A+I_B for the two schemes differ of less than 10 Gb/s. In particular, I_A=87.5 Gb/s, I_B=95 Gb/s (I_A+I_B=182.5 Gb/s) in the maximized scheme, and I_A=100 Gb/s, I_B=76 Gb/s (I_A+I_B=176 Gb/s) otherwise. In this figure are also reported simulations with LDPC codes with different code rates (the same applied in [13]), which best approach the achievable bound, showing that although some penalty must be taken into account, a good matching is evident. Each dot on the graph indicates the code rate of S_A and S_B respectively, in addition to the corresponding C/I. The reference BER for these LDPC simulations was equal to 10^{-4}, which corresponds to exceeding the code convergence threshold, and was measured on hundreds of 64800-bit transmitted codewords.

Fig. 10 focuses on the performance of S_A as a function of S_A OSNR and C/I when S_B is present or not, i.e. when the overlap technique was applied or not, in the case of the maximized scheme. Again, the curves present the theoretically-computed achievable bounds, while the dots report on the simulative results considering LDPC codes. Results show that when S_B is not present, I_A=100 Gb/s is achieved for S_A OSNR of 10 dB. When S_B is overlapped, in order to obtain I_A and I_B at 100 Gb/s, the $OSNR_{100}$=16.5 dB is required. The comparison between the theoretically-computed achievable bounds and the simulative results utilizing LDPC codes outlines a better matching when only S_A is present, as, predictably, the penalty is higher when the interfering channel is present. Indeed, such penalty depends on how conveniently the code characteristics fits with the channel, in fact the employed codes were designed for a memoryless AWGN channel. Therefore, a good code design is mandatory to obtain results close to the theoretical achievable bound (e.g.,

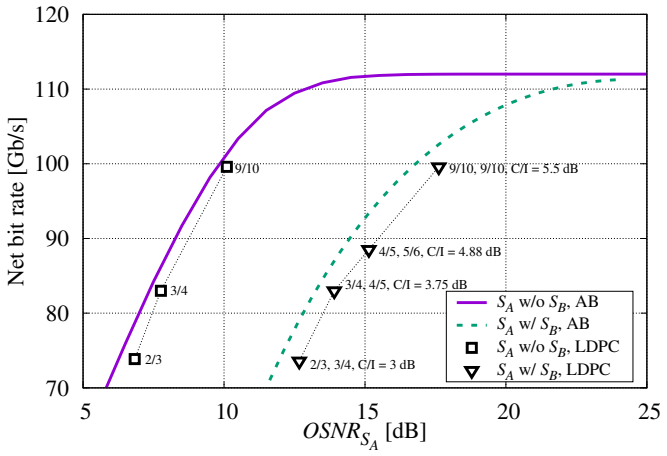

Figure 10. Net bit rate AB for channel S_A with channel S_B (maximized scheme) or without channel S_B, and LDPC codes simulations.

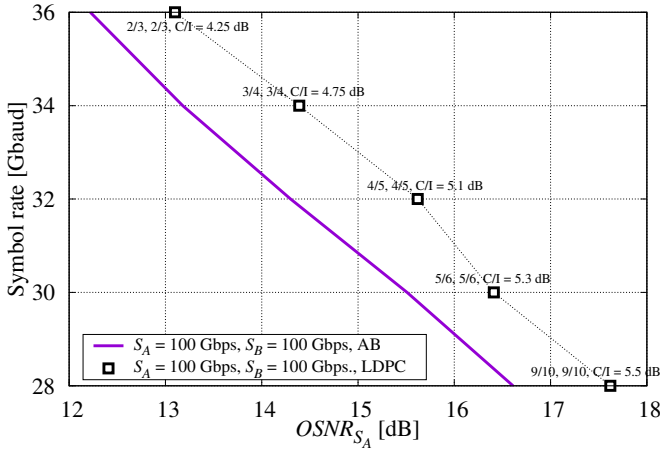

Figure 11. 100 Gb/s net bit rate for different symbol rates as a function of S_A OSNR, AB and LDPC codes simulations.

details on the design of LDPC codes can be found in [34], [35]).

Fig. 11 focuses on the scenario where 100 Gb/s of net bit rate has to be provided to the receiver on both overlapped signals, for different symbol rates. The transmitted gross rate was increased to values higher than 28 Gbaud, to assess the additional robustness achievable when larger overhead was introduced, at the expenses of a lower spectral efficiency. Results show that an OSNR improvement of around 2 dB can be achieved if the transmitted baud rate is increased to a value of 32 Gbaud.

Then, Fig. 12 and Fig. 13 show the effect of overlapping signals at different nodes along a dispersion-unmanaged link, in the absence and in the presence of nonlinear effects. The comparison was carried out by considering 50 spans of 80 km single-mode fiber (SMF) at maximum, and by choosing the overlap node for the different curves in the range from 0 to 50 spans, with a step size of 5 spans. Link parameters are summarized in Table II. Fiber dispersion is completely compensated for by the fixed-tap equalizer (see Fig. 6). S_A and S_B were assumed with I_A=I_B=100 Gb/s, 28 Gbaud symbol rate, and C_A=C_B=9/10, for the simulation points in Fig. 13. S_A was transmitted at a power level of 1 dBm whereas S_B at -4.5 dBm, i.e. with C/I=5.5 dB. The results of Fig. 12 were performed in the absence of nonlinear effects, and, as expected, a clear deterioration can be noticed as signals are overlapped

Parameter	value	Parameter	value
Numerical method	SSFM	Dispersion	16.63 ps/nm/km
SSFM step length	1 km	PMD	0 ps/$\sqrt{\text{km}}$
Sim. bandwidth	150 GHz	Attenuation	0.23 dB/km
Span length	80 km	Nonlinear coeff.	1.3 $(\text{W}\cdot\text{km})^{-1}$
EDFA noise figure	6 dB		

Table II. SIMULATED LINK PARAMETERS.

closer to the receiver, since the total noise increases with longer non-overlapped propagations (up to the case of overlapping just before the receiver, which corresponds to doubling the distance in terms of the accumulated noise). Interestingly, as shown in Fig. 13, when nonlinear effects come into play,[8] the performance loss due to variable overlapping node is almost negligible; this result can be explained with the fact that the performance deterioration in the copropagating path due to nonlinear effects is higher than in the single channel case, and thus the nonlinearities and AWGN accumulation have opposite effects. This fact has an important consequence, as it greatly simplifies the link characterization, by releasing the parameter setting dependence on the overlapping node. For example, any update of the results as in Fig. 3 could be simply reduced to a rigid translation of the curves. LDPC codes simulations confirm the predicted performance, as in the previous figures. The thin dashed lines in Fig. 13 introduce a 3-dB OSNR margin, thus reproducing a realistic transmission scenario accounting for practical code implementations and typical experimental degradations experienced in actual transmission systems.

For further information, in Fig. 13 the performance of 14-Gbaud 16-QAM is also reported. Indeed, two contiguous 14-Gbaud 16-QAM signals provide a nominal bit rate equal to the two considered overlapped QPSK signals and a frequency occupation approximately the same. As expected, the non-overlapped 16-QAM systems perform better in terms of optical reach. Results in Fig. 13 show that, for the bit rates of interest (i.e., equal or below 100 Gb/s) and with the considered C/I, the limiting optical reach is imposed by S_B. That is, the 100 Gb/s scenario is verified on the left region of the S_B curve. Results show that up to 800 km (on the 3-dB margin) can be successfully traversed by both overlapped signals with practical LDPC codes.

For larger distances, a degraded scenario is experienced. In particular, for distances lower than 1600 km, i.e., in the region at 100 Gb/s between the S_A and S_B curves, 100 Gbit/s for S_A can be provided. For example, for 1200 km, S_A successfully transmits 100 Gb/s while S_B still guarantees 95 Gb/s.

IV. CONCLUSIONS

A novel overlap technique was theoretically demonstrated and evaluated through simulations.

The technique allows two uncorrelated optical signals, transmitted along the same spectrum resources (i.e., overlapped), to be correctly detected. The technique relies on advanced coding technology, signal cancellation strategies and effective configuration of optical power levels.

The feasibility of the overlap technique has been already proved in a previous experimental demonstration.

In this study, the technique was first theoretically detailed.

Then, possible use cases of two overlapped 100 Gb/s PM-QPSK signals were considered.

[8] In this case the propagation was simulated through the Split-Step Fourier Method (SSFM), with proper step size (i.e. decreasing the step length until no performance change was noticed, which corresponds to approximately 1-km step length).

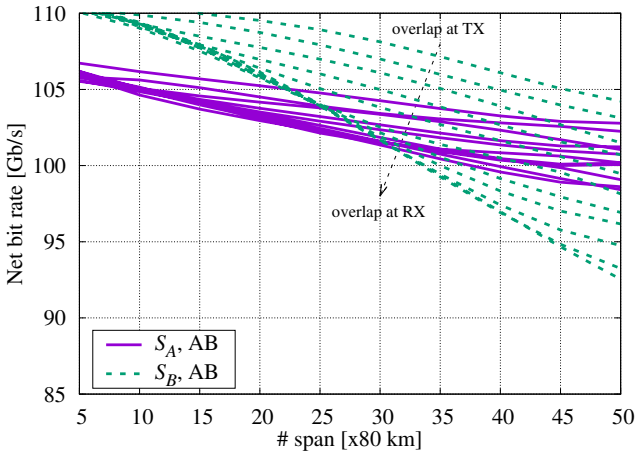

Figure 12. Net bit rate AB for channel overlap at different link nodes, in the absence of nonlinear effects.

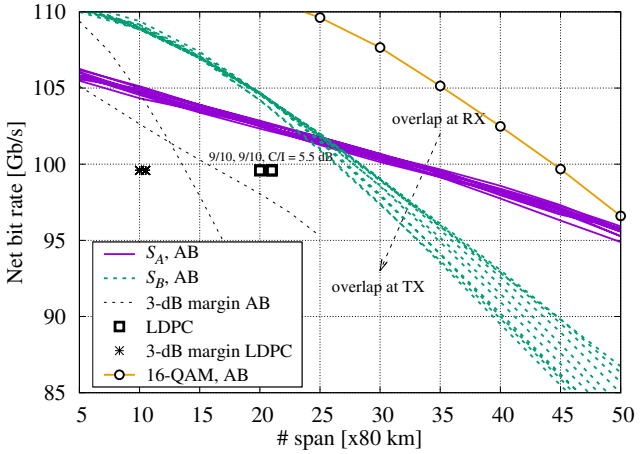

Figure 13. Net bit rate AB and LDPC codes simulations for channel overlap at different link nodes, and 14-Gbaud 16-QAM non-overlapped achievable bounds, in presence of nonlinear effects.

Two networking scenarios were addressed, where overlapped signals either (1) guarantee the full amount of bit rate at 100 Gb/s or (2) can admit a reduced net bit rate when longer optical reaches are needed. Simulation results were provided in terms of OSNR performance, showing the applicability conditions of the proposed technique in both networking scenarios. Results show that, when a 3-dB OSNR margin is applied on theoretical bounds, the proposed overlap technique successfully operates for optical reaches of up to 800km with 100 Gbit/s for each channel, whereas optical reaches can be more than doubled when 20% reduction of net bit rate is accepted.

The overlap technique requires adequate processing capabilities, with higher complexity than increasing the constellation size and using non overlapping frequency slots. In particular, the cancellation stage entails, apart from parameters estimation which can be performed quite slowly with respect to signalling rate, the remodulation of the first detected signal, which is basically the filtering of detected symbols; then, the subtraction of the remodulated signal must be carried out for each sample of the received overall signal. Therefore, the complexity of this processing is comparable with the complexity of the equalizer (including the estimation), and should be evaluated by considering that two signals can be detected with just one opto-electric front-end.

The proposed overlap technique, rather than representing a method for reaching higher values of spectral efficiency or longer distances, is proposed to enable potential networking use cases where the possibility of detecting two partially or totally overlapped signals can entail any advantages. Therefore, we used the spectral efficiency bounds as a figure of merit in order to show that signals can be successfully recovered and detected with specific performance, thus confirming the technique feasibility.

We believe that this technique should be seen as long-term solution, when the evolution of processing capabilities will relax implementation constraints. For this reason, it is not easy to predict which specific use cases are most promising for deployments. In this paper, we provided some examples on possible interesting use cases, like a defragmentation scheme and the 1+1 protection, which can be implemented thanks to the overlap technique and that are not achievable by increasing the constellation size with non overlapping frequency slots.

Future work is required to identify additional use cases and to elaborate on the proposed ones, verifying their applicability, feasibility and expected performance, and to address the technique viability with higher-order modulation formats.

ACKNOWLEDGMENT

The authors would like to thank P. J. Winzer for his valuable suggestions and fruitful discussions.

REFERENCES

[1] G. Meloni *et al.*, "First demonstration of optical signal overlap," in *Photonics in Switching (PS), Conf.*, 2014.

[2] D. Ly-Gagnon, S. Tsukamoto, K. Katoh, and K. Kikuchi, "Coherent detection of optical quadrature phase-shift keying signals with carrier phase estimation," *J. Lightwave Tech.*, vol. 24, no. 1, pp. 12–21, 2006.

[3] J. Renaudier *et al.*, "Generation and detection of 28 Gbaud polarization switched-QPSK in WDM long-haul transmission systems," *J. Lightwave Tech.*, vol. 30, no. 9, pp. 1312–1318, May 2012.

[4] F. Cugini *et al.*, "Demonstration of flexible optical network based on path computation element," *J. Lightwave Tech.*, vol. 30, no. 5, pp. 727–733, 2012.

[5] I. B. Djordjevic, M. Cvijetic, L. Xu, and T. Wang, "Using LDPC-coded modulation and coherent detection for ultra highspeed optical transmission," *J. Lightwave Tech.*, vol. 25, no. 11, pp. 3619–3625, 2007.

[6] N. Sambo *et al.*, "Programmable transponder, code and differentiated filter configuration in elastic optical networks," *J. Lightwave Tech.*, vol. 32, no. 11, pp. 2079–2086, June 2014.

[7] ITU-T G. 694.1, "Spectral grids for WDM application: DWDM frequency grid," Feb. 2012.

[8] Y. Li, D. King, F. Zhang, and A. Farrel, "Generalized labels for the flexi-grid in lambda-switch-capable (LSC) label switching routers," 2013. [Online]. Available: http://tools.ietf.org/html/draft-farrkingel-ccamp-flexigrid-lambda-label-06

[9] T. M. Cover and J. A. Thomas, *Elements of Information Theory*. New York: John Wiley & Sons, Inc., 1991.

[10] Y. Saito *et al.*, "Non-orthogonal multiple access (NOMA) for future radio access," *Proc. Vehicular Tech. Conf.*, Jun. 2013.

[11] P. J. Winzer, "An opto-electronic interferometer and its use in subcarrier add/drop multiplexing," *J. Lightwave Technol.*, vol. 31, no. 11, pp. 1775–1782, Jun 2013.

[12] A. Barbieri, D. Fertonani, and G. Colavolpe, "Time-frequency packing for linear modulations: spectral efficiency and practical detection schemes," *IEEE Trans. Commun.*, vol. 57, pp. 2951–2959, Oct. 2009.

[13] T. Foggi, G. Colavolpe, A. Bononi, and P. Serena, "Spectral efficiency optimization in flexi-grid long-haul optical systems," *J. Lightwave Tech.*, vol. 33, no. 11, pp. 2735–2742, Jul. 2015.

[14] L. Huang, S. Gao, and C.-K. Chan, "Wavelength conflict resolution by spectral overlap of two Nyquist-WDM signals," in *CLEO: 2015*. Optical Society of America, 2015.

[15] X. Wang, N. Wada, G. Cincotti, T. Miyazaki, and K. Kitayama, "Demonstration of over 128-Gb/s-capacity (12-user/spl times/10.71-Gb/s/user) asynchronous OCDMA using FEC and AWG-based multiport optical encoder/decoders," *IEEE Photon. Technol. Lett.*, vol. 18, no. 15, pp. 1603–1605, Aug 2006.

[16] W. Huang, M. H. M. Nizam, I. Andonovic, and M. Tur, "Coherent optical CDMA (OCDMA) systems used for high-capacity optical fiber networks-system description, OTDMA comparison, and OCDMA/WDMA networking," *J. Lightwave Tech.*, vol. 18, no. 6, pp. 765–778, June 2000.

[17] S. Verdú, *Multiuser Detection*. Cambridge, UK: Cambridge University Press, 1998.

[18] N. Kaneda, T. Pfau, and J. Lee, "Frequency diversity MIMO detection for coherent optical transmission," in *Proc. of ECOC 2013*, 2013.

[19] F. Hamaoka, K. Saito, T. Matsuda, and A. Naka, "Super high density multi-carrier transmission system by MIMO processing," in *Proc. of ECOC 2014*, 2014.

[20] G. Colavolpe and T. Foggi, "Time-frequency packing for high capacity coherent optical links," *IEEE Trans. Commun.*, vol. 62, no. 8, pp. 2986–2995, Aug. 2014.

[21] L. R. Bahl, J. Cocke, F. Jelinek, and J. Raviv, "Optimal decoding of linear codes for minimizing symbol error rate," *IEEE Trans. Inform. Theory*, vol. 20, pp. 284–287, Mar. 1974.

[22] G. Colavolpe and T. Foggi, "Next-generation long-haul optical links: higher spectral efficiency through time-frequency packing," in *Proc. IEEE Global Telecommun. Conf.*, Dec. 2013.

[23] D. M. Arnold, H.-A. Loeliger, P. O. Vontobel, A. Kavčić, and W. Zeng, "Simulation-based computation of information rates for channels with memory," *IEEE Trans. Inform. Theory*, vol. 52, no. 8, pp. 3498–3508, Aug. 2006.

[24] M. Klinkowski and K. Walkowiak, "Routing and spectrum assignment in spectrum sliced elastic optical path network," *IEEE Communications Letters*, vol. 15, no. 8, pp. 884–886, 2011.

[25] Y. Sone, A. Hirano, A. Kadohata, M. Jinno, and O. Ishida, "Routing and spectrum assignment algorithm maximizes spectrum utilization in optical networks," in *Proc. of ECOC 2011*.

[26] F. Cugini *et al.*, "Push-pull defragmentation without traffic disruption in flexible grid optical networks," *J. Lightwave Tech.*, vol. 31, no. 1, pp. 125–133, 2013.

[27] G. Mantelet *et al.*, "Establishment of dynamic lightpaths in filterless optical networks," *Journal of Optical Communications and Networking (JOCN)*, vol. 5, no. 9, pp. 1057–1065, 2013.

[28] B. Zaluski *et al.*, "Terastream implementation of all IP new architecture," in *MIPRO Conf.*

[29] Finisar Waveshaper. [Online]. Available: https://www.finisar.com/optical-instrumentation/waveshaper-16000s-multiport-optical-processor

[30] M. Secondini *et al.*, "Optical time-frequency packing: Principles, design, implementation, and experimental demonstration," *J. Lightwave Tech.*, vol. 33, no. 17, pp. 3558–3570, Jul. 2015.

[31] U. Mengali and M. Morelli, "Data-aided frequency estimation for burst digital transmission," *IEEE Trans. Commun.*, vol. 45, pp. 23–25, Jan. 1997.

[32] H. L. Van Trees, *Detection, Estimation, and Modulation Theory - Part I.* John Wiley & Sons, 1968.

[33] M. V. Eyuboglu and S. U. H. Qureshi, "Reduced-state sequence estimation with set partitioning and decision feedback," *IEEE Transactions on Communications*, vol. 36, no. 1, pp. 13–20, Jan. 1988.

[34] S. ten Brink, G. Kramer, and A. Ashikhmin, "Design of low-density parity-check codes for modulation and detection," *IEEE Trans. Commun.*, vol. 52, pp. 670–678, Apr. 2004.

[35] H. Xiao and A. H. Banihashemi, "Improved progressive-edge-growth (PEG) construction of irregular LDPC codes," *IEEE Commun. Letters*, vol. 8, pp. 715–717, Dec. 2004.